The Loop C Region of the Murine 5-HT_{3A} Receptor Contributes to the Differential Actions of 5-Hydroxytryptamine and *m*-Chlorophenylbiguanide†

Asha Suryanarayanan,‡,§ Prasad R. Joshi,‡,§ Zsolt Bikádi,|| Muthalagi Mani,⊥ Trupti R. Kulkarni,⊥ Chandra Gaines,⊥ and Marvin K. Schulte*,‡

Department of Chemistry and Biochemistry, The University of Alaska, Fairbanks, Alaska 99775, Department of Molecular Pharmacology, Institute of Chemistry, Chemical Research Center, P.O. Box 17, Budapest H-1525, Hungary, and Department of Basic Pharmaceutical Sciences, College of Pharmacy, The University of Louisiana, Monroe, Louisiana 71209

Received April 11, 2005; Revised Manuscript Received May 5, 2005

ABSTRACT: Sequence and predicted structural similarities between members of the Cys loop superfamily of ligand-gated ion channel receptors and the acetylcholine binding protein (AChBP) suggest that the ligand-binding site is formed by six loops that intersect at subunit interfaces. We employed site-directed mutagenesis to investigate the role of amino acids from the loop C region of the murine 5-HT_{3AS}R in interacting with two structurally different agonists, serotonin (5-HT) and *m*-chlorophenylbiguanide (*m*CPBG). Mutant receptors were evaluated using radioligand binding, two-electrode voltage clamp, and immunofluorescence studies. Electrophysiological assays were employed to identify changes in response characteristics and relative efficacies of *m*CPBG and the partial agonist, 2-methyl 5-HT (2-Me5-HT). We have also constructed novel 5-HT and *m*CPBG docked models of the receptor binding site based on homology models of the AChBP. Both ligand-docked models correlate well with results from mutagenesis and electrophysiological assays. Four key amino acids were identified as being important to ligand binding and/or gating of the receptor. Among these, I228 and D229 are specific for effects mediated by 5-HT compared to *m*CPBG, indicating a differential interaction of these ligands with loop C. Residues F226 and Y234 are important for both 5-HT and *m*CPBG interactions. Mutations at F226, I228, and Y234 also altered the relative efficacies of agonists, suggesting a role in the gating mechanism.

The serotonin type 3 receptor (5-HT_3R) is a member of the Cys loop superfamily of ligand-gated ion channel (LGIC) receptors that includes nicotinic acetylcholine, $GABA_A$, $GABA_C$, and glycine receptors (*1*). These receptors are membrane-bound ion channel-coupled receptors that mediate fast synaptic transmission in both peripheral and central nervous systems. 5-HT_{3A} subunits form homopentamers that yield characteristic inward currents with rapid onset and desensitization upon exposure to agonist. The ligand-binding site is present in the extracellular amino-terminal domain, at the subunit interface. 5-HT_{3A}R[1] antagonists are clinically used for the treatment of chemotherapy-induced emesis, and are being evaluated for several other conditions, including alcoholism (*2*).

Sequence and predicted structural similarities between LGIC receptors and the acetylcholine binding protein (AChBP) suggest that the ligand-binding site is formed by six loops, A−F, which intersect at the subunit interfaces (*3*−*6*). Several important residues in the 5-HT_{3A}R binding domain have been identified (*7*−*12*). Earlier work from our laboratory identified three important tyrosine residues (Y141, Y143, and Y153) in the loop E region (*13*). The development of AChBP-based homology models of the 5-HT_3R binding domain has also greatly improved our understanding of binding interactions of agonists and antagonists (*4*, *6*, *14*).

Previously, residues in the loop C region have been shown to contribute to interspecies differences in potencies of various ligands. The loop C region contributes to the higher potency of *d*-tubocurarine (*d*-TC) at the mouse 5-HT_3R compared to human receptors (*15*). This region has also been shown to contribute to the selective potency of 1-phenylbiguanide (PBG) at human 5-HT_3Rs (*16*). Similarly, the loop C region has been implicated in the higher potency of *m*-chlorophenyl biguanide (*m*CPBG) compared to serotonin (5-HT) at rat 5-HT_3Rs (*17*). 5-HT and *m*CPBG have been shown to exhibit distinct profiles on the murine 5-HT_{3A}R. Specifically, *m*CPBG exhibits a higher apparent affinity, slower association rates, and a higher affinity for the desensitized state compared to 5-HT (*18*−*20*). However, the molecular basis of these differences is not known. The primary focus of this study was to evaluate the interactions of 5-HT and *m*CPBG with each residue in the loop C region

† This work was supported by the National Science Foundation (NSF CAREER Grant 9985077), the American Heart Association (AHA Grant 0151065B), and Alaska INBRE (Grant P20 RR016466). A.S. and P.R.J. are Alaska INBRE graduate research fellows.

* To whom correspondence should be addressed: Department of Chemistry and Biochemistry, 146, Natural Sciences Facility, P.O. Box 756160, The University of Alaska, Fairbanks, AK 99775. Phone: (907) 474-5237. Fax: (907) 474-5640. E-mail: ffmks@uaf.edu.

‡ The University of Alaska.

§ These authors contributed equally to this work and are co-first authors.

|| Chemical Research Center.

⊥ The University of Louisiana.

[1] Abbreviations: 5-HT, serotonin; 5-HT_{3A}R, serotonin type 3A receptor; nAChR, nicotinic acetylcholine receptor; AChBP, acetylcholine binding protein; *m*CPBG, *m*-chlorophenylbiguanide; WT, wild type.

10.1021/bi050661e CCC: $30.25
Published on Web 06/01/2005

of the murine 5-HT$_{3A}$R using site-directed mutagenesis. Sequential alanine and/or conservative loop C mutations were characterized by radioligand binding and electrophysiological assays. Mutants that ablated binding and/or function were further characterized by immunofluorescence assays. Experimental data were correlated with ligand docking calculations for both 5-HT and *m*CPBG obtained from an AChBP-based homology model of the murine 5-HT$_{3A}$R. Taken together, results presented here reveal an emerging picture of differential interaction and gating of the 5-HT$_3$R by 5-HT and *m*CPBG.

MATERIALS AND METHODS

[^{3}H]Granisetron was purchased from New England Nuclear (NEN). 5-HT and 2-Me5-HT were obtained from Spectrum, and *m*CPBG was obtained from Research Biochemical International. *Xenopus laevis* frogs and frog food were obtained from Xenopus Express. Sigma type II collagenase was purchased from Sigma Aldrich. All other chemicals were purchased from Fisher Scientific.

Site-Directed Mutagenesis and Epitope Tagging. Site-directed mutagenesis was performed as described previously (*13*), using either the QuickChange mutagenesis kit (Stratagene) or the pAlter altered sites mutagenesis kit (Promega). Wild-type (WT) 5-HT$_{3AS}$ cDNA was derived from N1E-115 neuroblastoma cells and cloned in the pCI vector as described previously (*12*). For immunofluorescence studies, FLAG-tagged receptors were used. A C-terminal FLAG epitope tagged receptor was created by cloning the WT cDNA into the pCMV 4.1 vector (Stratagene). This WT-FLAG cDNA was then used as a template to create the FLAG-tagged F226A, S233A, and Y234A mutations using the QuickChange mutagenesis kit. All constructs were confirmed by restriction digests and DNA sequencing (University of California, Davis, CA).

*Cell Culture and Transient Transfection. t*SA 201 cells (a derivative of HEK 293 cells) were obtained from M. White (*12*). *t*SA 201 cells were cultured in Dulbecco's modified Eagle's medium (DMEM, New Life Technologies) supplemented with 10% fetal bovine serum and 100 units/mL penicillin/streptomycin in a humidified 5% CO_2 atmosphere at 37 °C. For radioligand binding studies, *t*SA 201 cells were plated on 90 mm culture dishes at a density of 5×10^6 cells/dish and grown for 9 h prior to transfection. The cells were transfected with 20 μg of WT or mutant plasmid DNA per dish using a calcium phosphate transfection kit (New Life Technologies). Transfected cells were supplemented with fresh DMEM 12−15 h after transfection and harvested 36 h later.

Radioligand Binding Assays. Radioligand binding assays were performed as described previously (*13*). Briefly, transfected cells were scraped from the dishes, washed twice with phosphate buffered saline (PBS, New Life Technologies), and then resuspended in 1.0 mL of PBS with protease inhibitor cocktail/100 mm dish (Complete Protease Inhibitor Cocktail, Roche, Mannheim, Germany). Immediately prior to use, cells were homogenized in PBS with protease inhibitors using a glass tissue homogenizer, centrifuged, washed, and resuspended in 1 mL of PBS/100 mm dish. The protein content was determined using Lowry assay (Sigma Diagnostics). Binding assays were performed in PBS with protease inhibitors. For K_d determinations, 50 μL of homogenate was incubated at 37 °C for 1 h with varying concentrations of [^{3}H]granisetron. The level of specific binding of [^{3}H]granisetron was determined as the amount of bound [^{3}H]granisetron not displaced by a saturating concentration of a competing ligand (10 μM Tropisetron). For K_i determinations, 50 μL of homogenate was incubated at 37 °C for 2 h with varying concentrations of inhibitor and [^{3}H]granisetron (NEN). Binding was terminated by rapid filtration onto GF/B filters.

Electrophysiology. Details of the vertical perfusion chamber and methodology employed for electrophysiological recordings have been described previously (*21*). Briefly, ovarian lobes were surgically removed from *Xenopus laevis* frogs, washed twice in Ca^{2+} free Barth's buffer [82.5 mM NaCl, 2.5 mM KCl, 1 mM $MgCl_2$, and 5 mM HEPES (pH 7.4)] and gently shaken with 1.5 mg/mL collagenase (Sigma type II, Sigma-Aldrich) for 1 h at 20−25 °C. Stage IV oocytes were selected for microinjection. Synthetic cRNAs for WT and mutant mouse 5-HT$_{3As}$ receptors were prepared using the mMESSAGE mMACHINE High Yield Capped RNA Transcription Kit (Ambion). Each oocyte was injected with 50 nL of cRNA at a concentration of 0.2 ng/nL. Oocytes were incubated at 19 °C for 2−4 days before electrophysiological recording. Electrical recordings were made under conventional two-electrode voltage clamp conditions using an OC-725C oocyte clamp amplifier (Warner Instruments) coupled to an online, computerized data acquisition system (Datapac 2000, RUN technologies). Recording and current electrodes were filled with 3 M KCl and had resistances of 1−2 MΩ. Oocytes were held in a vertical flow chamber with a volume of 400 μL and perfused with ND-96 recording buffer [96 mM NaCl, 2 mM KCl, 1.8 mM $CaCl_2$, 1 mM $MgCl_2$, and 5 mM HEPES (pH 7.4)] at a rate of 15 mL/min. All agonists were prepared in ND-96 buffer and applied at a rate of 25 mL/min using an electrical pump.

Maximal currents elicited by each agonist were recorded using saturating (supramaximal) concentrations of the agonist. 5-HT was assumed to be the full agonist based on data obtained for the WT receptor. The relative efficacy of an agonist (relative to 5-HT) was calculated as $I_{\text{max agonist}}/I_{\text{max 5-HT}}$. For each experiment, maximal currents elicited by *m*CPBG and 2-Me5-HT were compared (normalized) to the maximal current elicited by 5-HT on the same oocyte. Such comparisons were repeated on four or more oocytes for WT and mutant receptors. All the normalized data were pooled together to calculate relative efficacy values ± the standard error.

Localization of WT and Mutant 5-HT$_3$Rs by Immunofluorescence. WT-FLAG (WT 5-HT$_{3A}$R with a C-terminal FLAG tag), F226A-FLAG, S233A-FLAG, and Y234A-FLAG were characterized by immunofluorescence in *t*SA 201 cells. *t*SA 201 cells transiently expressing either the WT or mutant 5-HT$_3$Rs were grown in chamber slides in DMEM at 37 °C; 24−28 h post transfection, chamber slides were washed thrice with PBS and incubated in freshly prepared ice-cold 4% paraformaldehyde in PBS to fix the cells. The chamber slides were then incubated with an anti-FLAG antibody (Sigma) at a dilution of 1:200 in PBS for 1 h at room temperature (RT). To determine the level of intracellular expression, cells were permeabilized by incubation with primary anti-FLAG antibody diluted in 0.3% Triton X-100. After three PBS washes of 5 min each, slides were incubated for 1 h at RT

with goat anti-mouse rhodamine-conjugated secondary antibody (Jackson ImmunoResearch) diluted at 1:1000 in PBS. After three PBS washes, slides were mounted and observed under a Nikon upright microscope with appropriate filters. The cells were viewed under a 20× objective and photographed using a Cool Snap digital camera attached to the microscope. Polymorph software was used to acquire digital photographs.

Receptor Modeling. Extracellular regions of the homopentameric murine 5-HT_3R were built on the basis of the crystal structure of AChBP from the snail *Lymnaea stagnalis* (PDB entry 1I9B). The sequence of the 5-HT_3R A subunit was taken from Protein Information Resource (*22*) entry NF00508262. Multiple-sequence alignments of their extracellular regions and AChBP were performed with ClustalW using default parameters (*23*). On the basis of this alignment, homology model building of the 5-HT_{3A}R subunit was carried out using the "Nest" and "Loopy" facility of the Jackal protein structure modeling package. Nest predicts the experimental dihedral angles χ_1 within an error range of 20° for 94% of protein side chains (*24*). Protein loop predictions for amino acid insertions and deletion were carried out with Loopy (*25*). Heterodimeric units of the pentamer were built on the basis of crystal structure data to reach minimal root mean standard deviation (rmsd) between the matched monomers. Further refinements of the resulting dimers were carried out with Sybyl version 6.6 (Tripos Inc., St. Louis, MO) on a Silicon Graphics Octane workstation under an Irix 6.5 operation system. The all-atom model was allowed to relax during a short molecular dynamics run using constrains for backbone atoms. Finally, the entire structures were fully minimized without any restriction using the Powell conjugate gradient method until the maximum derivative was less than 0.050 kcal mol^{-1} $Å^{-1}$. Gasteiger−Huckel partial charges were applied during the calculations. The quality of the model was verified using Procheck, as compared with well-refined structures at the same resolution (*26*). Intra- and interface H-bonds were analyzed with HBPLUS version 3.0, a hydrogen bond calculation program (*27*).

Ligand Docking. Ligand docking was performed independent of the experimental data; i.e., no constraints based on the experimental data were applied. AutoDock version 3.0 (*28*) was applied for docking calculations, using the Lamarckian genetic algorithm (LGA) and the "pseudo-Solis and Wets" (pSW) methods. The parameters included in AutoDock are based on the "Assisted Model Building with Energy Refinement" (AMBER) force field (*29*). Gasteiger−Huckel partial charges were applied both for ligands and proteins. Solvation parameters were added to the protein coordinate file, and the ligand torsions were defined using the "Addsol" and "Autotors" utilities, respectively, in AutoDock version 3.0. The atomic affinity grids were prepared with 0.375 Å spacing using the Autogrid program for a 15 Å × 15 Å × 22.5 Å box around the interface of subunits. Random starting positions, orientations, and torsions (for flexible bonds) were used for the ligands. Each docking run consisted of 100 cycles. The number of evaluations was set to 1.5 million. Final structures with an rmsd of less than 1.5 Å were considered to belong to the same cluster. The structures with low energies and high frequencies of docking were subjected to a further minimization with Sybyl and were examined.

```
                    224   AAAAAAAAA   A  236
m 5-HT3AS             K--EFSIDISNS---YAE
m 5-HT3B              H--IRQSSA-GD---FAQ
h 5-HT3A              R--EFSMESSNY---YAE
h 5-HT3B              S--ILQSSAGG----FAQ
Torpedo nACh alpha    HWVYYTCCPDTP---YLD
m nACh alpha          HWVFYSCCPTTP---YLD
AChBP                 NSVTYSCCPEA----YED
m GABAA alpha 1       GIVQSSTG------EYVV
m GABAA beta 1        KKVEFTTG------AYPR
r GABAA beta 2        KKVVFSTG------SYPR
m Gly alpha 1         Y--CTKHYN---TGKFTC
```

FIGURE 1: Sequence alignment of the purported loop C region of the 5-HT_{3AS} receptor with other members of the family. The amino acid sequence of the mouse 5-hydroxytryptamine type 3A short isoform receptor (m 5-HT_{3AS}R) was aligned with sequences of other ligand gated ion channel receptors and the acetylcholine binding protein (AChBP) using a multisequence ClustalX alignment method. The alignment of the purported "loop C" region across various members of the LGIC superfamily and the AChBP is shown. Conserved residues are bold and highlighted in gray. Residues found to be important in this study are bold and italicized in the mouse 5-HT_{3AS}R. The numbers at the end indicate the positions as measured from the N-terminus, including the initial methionine in the protein sequence of the mouse 5-HT_{3AS}R. Residues in the mouse 5-HT_{3AS}R that are mutated to alanines are denoted with an A above each WT residue.

Data Analysis. Radioligand binding data were analyzed as follows. K_d values were determined by fitting the binding data, using GraphPad (San Diego, CA) PRISM, to the equation $B = (B_{max}[L]^n)/([L]^n + K^n)$, where B is the amount of specifically bound ligand, B_{max} is the maximum level of binding at equilibrium, L is the free ligand concentration, K is the equilibrium dissociation constant, and n is the Hill coefficient.

IC_{50} values were calculated by fitting the data, using GraphPad PRISM, to the equation $\theta = 1/(1 + L/IC_{50})$, where θ is the fractional amount of [^{3}H]granisetron bound in the presence of inhibitor at concentration L compared to the amount of [^{3}H]granisetron bound in the absence of inhibitor. IC_{50} is the concentration at which $\theta = 0.5$. K_i values were calculated from IC_{50} values using the Cheng−Prusoff equation.

Dose−response curves obtained from electrophysiological data were fit using the equation $I = I_{max}/(1 + EC_{50}/[A]^n)$, where I is the current at a given agonist concentration, I_{max} is the maximal current, EC_{50} is the agonist concentration that elicits a half-maximal current, and n is the Hill coefficient. The significance of results ($p < 0.05$) was determined with a Student's t test in GraphPad PRISM.

RESULTS

Radioligand Binding Studies. A sequence comparison between the putative C loop of representative members of the Cys loop LGIC superfamily is shown in Figure 1. The amino acid sequence from E225 to E236 of the murine 5-HT_{3AS}R is shown in the top row. Amino acids from E225 to Y234 were individually mutated to alanine in this study. Mutations with R group characteristics more similar to those of the WT residue (conservative mutations) were made if the initial alanine mutation showed no binding and/or function. The WT and mutant 5-HT_{3A}Rs were expressed in *t*SA 201 cells and evaluated by saturation and competition radioligand binding assays. The results are summarized in

Table 1: Effects of Loop C Mutations on 5-HT$_{3A}$R Radioligand Binding[a]

	[^{3}H]granisetron				5-HT		mCPBG	
receptor	B_{max} (pmol/mg)	K_d (nM)	n_H	*x*-fold change	K_i (μM)	*x*-fold change	K_i (μM)	*x*-fold change
WT	12.60 ± 0.23	0.98 ± 0.12	1.20 ± 0.08	1	0.16 ± 0.04	1	0.10 ± 0.02	1
E225A	10.80 ± 1.31	4.25 ± 0.44[b]	1.41 ± 0.12	4	1.70 ± 0.04[b]	10	0.14 ± 0.04	1.4
F226A	18.40 ± 1.29[b]	1.36 ± 0.16	1.37 ± 0.14	1.4	32.6 ± 2.9[b]	200	3.9 ± 0.63[b]	40
F226Y	14.40 ± 1.19	2.09 ± 0.04	1.28 ± 0.08	2	29.7 ± 3.8[b]	185	2.8 ± 0.6[b]	28
I228A	15.4 ± 2.0	4.65 ± 0.40[b]	1.53 ± 0.14	4.5	37.7 ± 2.7[b]	235	0.52 ± 0.04[b]	5
D229A	10.5 ± 0.7	8.13 ± 0.18[b]	1.20 ± 0.09	8	22.2 ± 2.6[b]	140	0.27 ± 0.03	2.5
S233A	–	–	–	–	–	–	–	–
S233T	15.90 ± 1.22	2.04 ± 0.19	1.31 ± 0.12	2	0.66 ± 0.05[b]	4	0.12 ± 0.02	1
Y234A	–	–	–	–	–	–	–	–
Y234F	10.20 ± 1.13	11.20 ± 0.61[b]	1.40 ± 0.09	11	30.0 ± 1.2[b]	185	12.40 ± 1.32[b]	125

[a] Ligand affinities of WT and mutant receptors were determined using either saturation binding assays with [^{3}H]granisetron or competition assays (for serotonin and *m*CPBG) as described in Materials and Methods. Expression levels of receptors are indicated as B_{max} values. Each value was obtained using at least four determinations at each concentration, and is reported as the mean ± the standard error. Dashes for S233A and Y234A indicate that values could not be determined since no specific binding to [^{3}H]granisetron could be detected. [b] Significantly different from the WT value ($p \leq 0.05$).

Table 2: Effects of Loop C Mutations on 5-HT$_{3A}$R Electrophysiology[a]

	5-HT				*m*CPBG			
receptor	EC_{50} (μM)	n_H	*x*-fold change	I_{max}(5-HT) (μA)	EC_{50} (μM)	n_H	*x*-fold change	I_{max}(*m*CPBG) (μA)
WT	3.41 ± 0.40	1.40 ± 0.19	1	14.8 ± 2.2	0.78 ± 0.07	1.61 ± 0.20	1	13.7 ± 1.8
E225A	10.80 ± 1.50[b]	1.50 ± 0.10	3.2	6.2 ± 0.8[b]	2.26 ± 0.23[b]	1.40 ± 0.18	3	5.9 ± 1.1[b]
F226A	–	–	–	–	–	–	–	–
F226Y	25.21 ± 1.11[b]	2.58 ± 0.31[b]	7.4	0.5 ± 0.2[b]	6.62 ± 0.63[b]	2.14 ± 0.30	8.5	0.8 ± 0.2[b]
I228A	34.00 ± 2.00[b]	2.00 ± 0.20	10	0.5 ± 0.1[b]	12.30 ± 1.20[b]	1.40 ± 0.18	16	13.5 ± 1.5
D229A	42.91 ± 2.34[b]	1.41 ± 0.09	12.5	11.2 ± 1.4	1.37 ± 0.02	2.50 ± 0.07	1.8	10.4 ± 1.1
S233A	–	–	–	–	–	–	–	–
S233T	2.33 ± 0.13	1.51 ± 0.12	−1.5	15.2 ± 1.8	0.48 ± 0.04	1.29 ± 0.12	−1.6	14.0 ± 1.6
Y234A	–	–	–	–	–	–	–	–
Y234F	9.17 ± 0.44[b]	2.87 ± 0.62[b]	2.7	13.3 ± 1.5	5.7 ± 0.2[b]	2.12 ± 0.09	7.3	16.8 ± 1.9

[a] EC_{50} and Hill coefficient values of serotonin and *m*CPBG for WT and mutant receptors were determined from dose−response curves of electrophysiological data as described in Materials and Methods. Each value was obtained using at least four determinations at each concentration, and is reported with the standard error. I_{max} values indicate average maximal currents elicited by the agonist for the respective receptor. Dashes indicate that the values could not be determined since the receptor was not functional. [b] Significantly different from the WT value ($p \leq 0.05$).

Table 1. All mutant receptors except S233A and Y234A bound [^{3}H]granisetron. The B_{max} values for all mutant receptors that bound [^{3}H]granisetron were comparable to that of WT receptors. Small changes in the K_d value of [^{3}H]-granisetron were seen for E225A and I228A receptors compared to the WT receptor. Larger changes in K_d were noted for D229A and Y234F receptors.

Competition binding assays were carried out to determine the affinity of agonists, 5-HT and *m*CPBG. The fold changes in affinity of 5-HT and *m*CPBG for mutant receptors compared to those of WT receptors are shown in Table 1. 5-HT affinity was significantly decreased by all mutations that were tested with the largest changes observed for mutations at F226, I228, D229, and Y234. *m*CPBG affinity was significantly reduced by mutations at only F226, I228, and Y234. Throughout the entire loop, K_i values for 5-HT were more significantly altered than those of *m*CPBG.

Electrophysiological Studies. Table 2 summarizes the electrophysiological characterization of WT and mutant receptors using two electrode voltage clamp assays in *Xenopus* oocytes. Representative traces of currents elicited upon application of supramaximal levels of 5-HT, *m*CPBG, and the partial agonist 2-Me5-HT are shown in Figure 2. These traces represent currents recorded from the same oocyte, hence from the same number (population) of receptors. No currents could be elicited upon application of 5-HT or *m*CPBG in oocytes injected with either S233A or Y234A mRNA. The lack of detectable currents in these mutants correlates with the lack of [^{3}H]granisetron binding observed in radioligand binding assays. Small changes in EC_{50} were seen for the E225A mutation. Surprisingly, no currents could be elicited from oocytes injected with the F226A mRNA, whereas F226A receptors showed robust binding to [^{3}H]-granisetron. The conservative F226Y mutation showed a 7−8-fold change in EC_{50} values of both 5-HT and *m*CPBG, accompanied with drastic changes in response kinetics and I_{max} values compared to those of WT (Figure 2). These changes in EC_{50} values are also paralleled by large decreases in affinities of 5-HT and *m*CPBG in binding assays (Table 1). The I228A mutation also showed large changes in EC_{50} values of both agonists. Interestingly, this mutation causes selective changes in currents mediated by 5-HT, and not by *m*CPBG, as reflected by the representative traces in Figure 2. The $I_{max\ mCPBG}$ for I228A receptors remains similar to those obtained for WT receptors. A similar selectivity is also seen in competition assays of this receptor where the K_i value of 5-HT but not *m*CPBG is altered (Table 1). The D229A mutation produced the largest increase in the EC_{50} value for 5-HT. However, no significant change was seen in the EC_{50} value for *m*CPBG. In parallel to these results, D229A receptors produced a large increase in the K_i value for 5-HT and not for *m*CPBG in competition assays. In contrast to mutations at F226, I228, and D229, the Y234F mutation produced a small change in the EC_{50} value for 5-HT and a

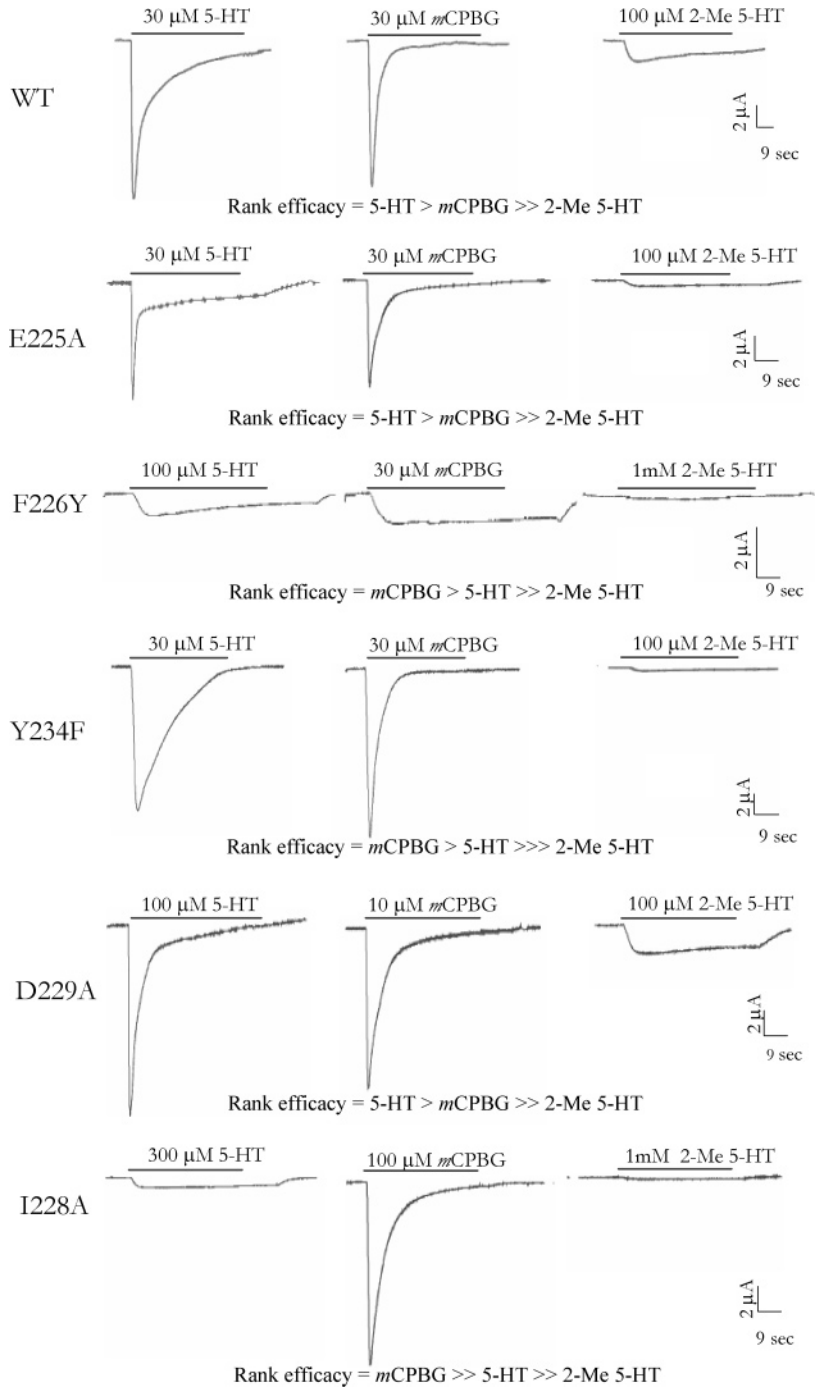

FIGURE 2: Electrophysiological characterization of WT, E225A, F226Y, I228A, D229A, and Y234F receptors expressed in *Xenopus laevis* oocytes. Characteristics of inward currents elicited by application of agonists at supramaximal concentrations are shown for each receptor type. All traces shown for a particular receptor were obtained from the same oocytes and are representative of multiple experiments ($n \geq 4$). The solid bar at the top of each trace denotes the time of drug exposure, the type of agonist used, and its concentration. The rank efficacy for each receptor type is also shown.

larger change in the EC_{50} value for *m*CPBG. However, Y234F receptors show large changes in the K_i value for both agonists in competition assays.

K_d, K_i, and EC_{50} measurements for a mutant receptor indicate that the mutated amino acid is potentially important. However, these data alone cannot distinguish between a role in binding or transduction of the binding signal that causes the channel to open, i.e., gating (*30*). To further characterize the residues that exhibited significant changes in binding and/or electrophysiological assays, we employed the partial agonist approach (*31*−*35*). In this approach, maximal currents (I_{max}) of full and partial agonist are compared on a single receptor preparation for both WT and mutant receptors. Assuming that the single-channel conductance and the desensitization rates remain unchanged, measurement of fractional I_{max} ratios (relative efficacies) can be used to indicate changes in the gating constant *E* (*36*). We have employed the 5-HT_3R partial agonist, 2-methyl 5-HT (2-Me5-HT), since it has ∼12% relative efficacy (0.120 ± 0.002) as compared to that of the full agonist, 5-HT. A mutation affecting gating should result in an easily detectable change in the relative efficacy of 2-Me5-HT compared to

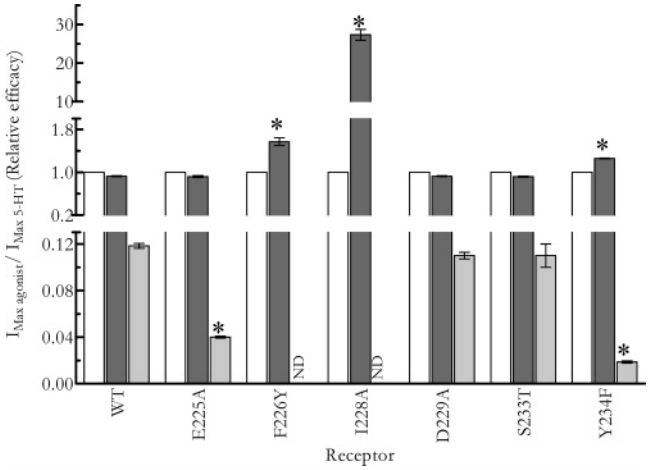

FIGURE 3: Changes in relative efficacies of 2-Me5-HT and *m*CPBG for WT and mutant receptors. This bar graph shows a comparison of $I_{max\ agonist}/I_{max\ 5-HT}$ (relative efficacy) for WT and mutant receptors. For each receptor type, maximal currents elicited by each agonist (*m*CPBG and 2-Me5-HT) were directly compared to those elicited by 5-HT on a single oocyte. Results are from such multiple experiments. Error bars indicate the standard error. White bars depict data for 5-HT, dark gray bars data for *m*CPBG, and light gray bars data for 2-Me5-HT. The relative efficacy of 5-HT is 1.00 for each receptor type since currents for all agonists were normalized to $I_{max\ 5-HT}$. For WT receptors, the relative efficacies of *m*CPBG and 2-Me5-HT were 0.93 ± 0.01 and 0.12 ± 0.002, respectively, yielding the following rank efficacy: 5-HT > *m*CPBG ≫ 2-Me5-HT (Figure 2). Changes in rank efficacy for mutant receptors (shown in Figures 2 and 3) are reflected in this bar graph. Asterisks denote values significantly different from that of WT ($p \leq 0.05$). ND indicates the relative efficacy of 2-Me5-HT could not be detected.

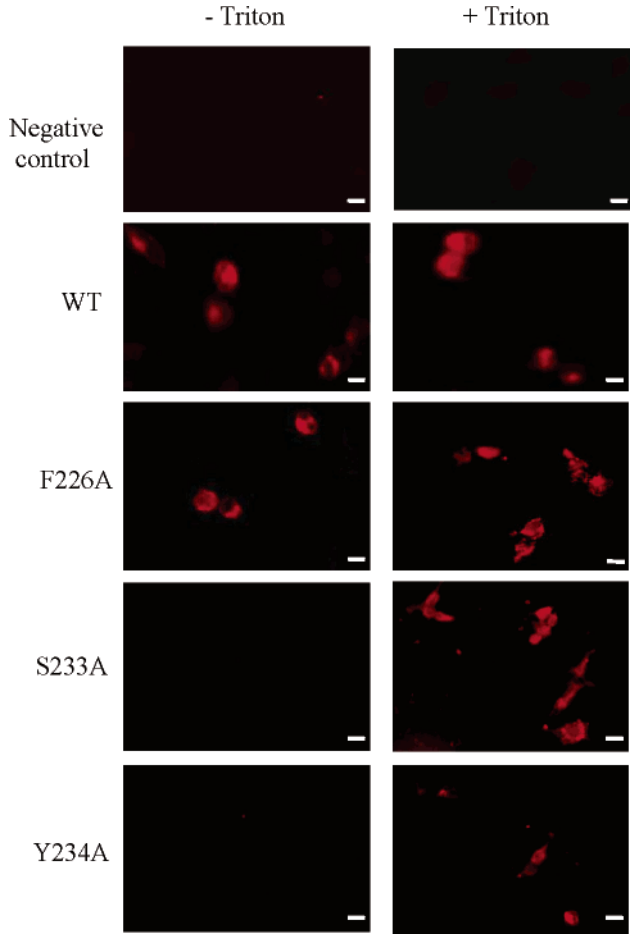

FIGURE 4: Localization of C-terminal FLAG-tagged WT and loop C mutant receptors by immunofluorescence. To determine the presence of WT and mutant receptors on the cell surface, FLAG-tagged WT or mutant receptors were transiently expressed in *t*SA 201 cells and characterized using immunofluorescence. Fixed cells were initially incubated with an anti-mouse anti-FLAG primary antibody. Intracellular localization was assessed using Triton X-100. Cell surface or intracellular localization was assessed by using an anti-goat rhodamine-conjugated secondary antibody. All images were acquired using a 20× magnification lens coupled to a digital camera. The scale bar is 10 μm. The first column shows the localization in absence of Triton, and the second column shows the localization in the presence of Triton, i.e., permeabilized cells. A negative control (i.e., cells transfected with the empty pCMV 4.1 vector, no primary antibody added) with and without Triton is also included at the top.

that of 5-HT ($I_{max\ 2-Me5-HT}/I_{max\ 5-HT}$). To compare fractional maximal currents (relative efficacies) for all agonists (5-HT, *m*CPBG, and 2-Me5-HT), the fractional I_{max} value obtained for 5-HT was assumed to be 100% or 1.00 for each receptor. This assumption is solely used as a reference for I_{max} comparisons. Significant changes in relative efficacies and rank efficacies for a mutant receptor as compared to that of the WT receptor would thus suggest a role in gating.

We determined rank efficacies of 5-HT, *m*CPBG, and 2-Me5-HT on WT and mutant receptors (Figure 2). Relative efficacy values obtained for *m*CPBG ($I_{max\ mCPBG}/I_{max\ 5-HT}$) and 2-Me5-HT ($I_{max\ 2-Me5-HT}/I_{max\ 5-HT}$) are summarized in Figure 3. The EC_{50} value of 2-Me5-HT was 16.4 ± 1.1 μM for WT. The rank efficacy observed for WT receptors was as follows: 5-HT > *m*CPBG ≫ 2-Me5-HT (Figure 2). In comparison to that of 5-HT, the relative efficacy of *m*CPBG ($I_{max\ mCPBG}/I_{max\ 5-HT}$) was 0.93 ± 0.01, while that of 2-Me5-HT ($I_{max\ 2-Me5-HT}/I_{max\ 5-HT}$) was 0.120 ± 0.002 (Figure 3). As shown in the bar graph in Figure 3, a significant decrease in the relative efficacy of 2-Me5-HT was observed for E225A (0.04 ± 0.001) and Y234F (0.019 ± 0.001) receptors compared to WT (0.120 ± 0.002). The relative efficacy of 2-Me5-HT at F226Y and I228A receptors could not be determined since application of 1 mM 2-Me5-HT could not elicit detectable responses in either receptor (Figure 2). Given the extremely low $I_{max\ 5-HT}$ values for these mutant receptors, the relative efficacy of 2-Me5-HT would be expected to be very significantly reduced for F226Y and I228A receptors compared to that of WT. The relative efficacy of *m*CPBG was significantly altered for F226Y (1.57 ± 0.07), I228A (27.33 ± 1.39), and Y234F (1.26 ± 0.007) receptors compared to that of WT (0.92 ± 0.018). These data suggest that E225, F226, and Y234 play a role in gating of the murine 5-HT$_{3A}$R. In addition, mutation of I228 selectively alters gating by 5-HT but not by *m*CPBG. No change in the relative efficacy of either 2-Me5-HT or *m*CPBG was observed for D229 and S233T receptors, indicating that these residues do not play a role in gating.

Immunofluorescence Studies. Immunofluorescence studies were carried out for WT-FLAG receptors and mutant receptors that ablated binding and/or function. Results obtained for tagged WT and mutant receptors are shown in Figure 4. A strong signal is obtained for WT-FLAG receptors in the absence of detergent (Triton), indicating cell surface expression. In addition, permeabilized cells show WT receptors located intracellularly, in the process of either assembly or transport to the cell membrane. Data for F226A

receptors show that they are expressed on the cell surface. However, S233A and Y234A receptors are not expressed on the cell surface. Fluorescence was detected in permeabilized cells transfected with either S233A or Y234A cDNA, indicating either incompletely or incorrectly assembled subunits that remain intracellularly located. These data suggest that S233A and Y234A mutations affect receptor assembly and/or trafficking to the cell membrane.

Docking of 5-HT, mCPBG, and 2-Methyl 5-HT to the Murine 5-HT$_{3A}$R Model. To further investigate the differential interactions of 5-HT and *m*CPBG that we observed in radioligand binding and electrophysiological studies, we carried out docking studies using an AChBP-based model of the murine 5-HT$_{3A}$R. Figure 5 shows docking of 5-HT and *m*CPBG to this model. No constraints based on the experimental data were applied while performing these docking calculations. All ligands are docked in the binding cavity previously described for 5-HT$_3$Rs (*6*, *14*). The presence of both aromatic (W90, W183, Y143, Y153, Y234, and F226) and acidic residues (E225, E236, and D229) at the binding interface suggests that basic ligands can form cation$-\pi$ interactions and salt bridges. The interactions are also highlighted in Table 3.

The most frequent docking position of 5-HT (Figure 5A) forms interactions similar to that observed for the second *m*CPBG docking model. The amino group of 5-HT is intercalated between the aromatic F226 and Y234 residues, while it is salt bridged with E236. The aromatic ring of 5-HT is involved in a $\pi-\pi$ interaction with W183. The hydroxyl group forms a hydrogen bond with D229. The docking calculations for 2-Me5-HT are similar to those for 5-HT, with the only point of difference being Y234, which forms a hydrogen bond with 2-Me5-HT.

The docking calculations resulted in two possible models for *m*CPBG with nearly equal energies. The first model of *m*CPBG binding ("1") is shown in Figure 5B. In this case, the guanidino group forms a salt bridge with D229. Y153 and Y234 can form hydrogen bonds and/or are involved in cation$-\pi$ interaction with the guanidino group. W183 is also part of this aromatic pocket. The chloro group of *m*CPBG is near F226 in this model. The following interactions occur in the second model, "2" (Figure 5C). The guanidino group forms a salt bridge with E236, while it is also involved in a cation$-\pi$ interaction with F226 and Y234. The aromatic ring of *m*CPBG lies nearly parallel to W183, producing weak $\pi-\pi$ interaction. W90 is also in the proximity of the aromatic ring and the chloro group.

A comparison of 5-HT and *m*CPBG docked models reveals that interactions in the 5-HT docked model are similar to those observed for the second *m*CPBG docking model (Table 3). However, two critical differences in the interactions of these agonists can be noted. First, the OH group of 5-HT is able to form a hydrogen bridge with D229. D229 does not form an interaction with *m*CPBG in model 2, while it forms a salt bridge interaction in model 1. Second, Y153 (a loop E residue) is within 4 Å of docked 5-HT in the 5-HT model, while it forms a hydrogen bond with *m*CPBG in model 1 and does not in model 2.

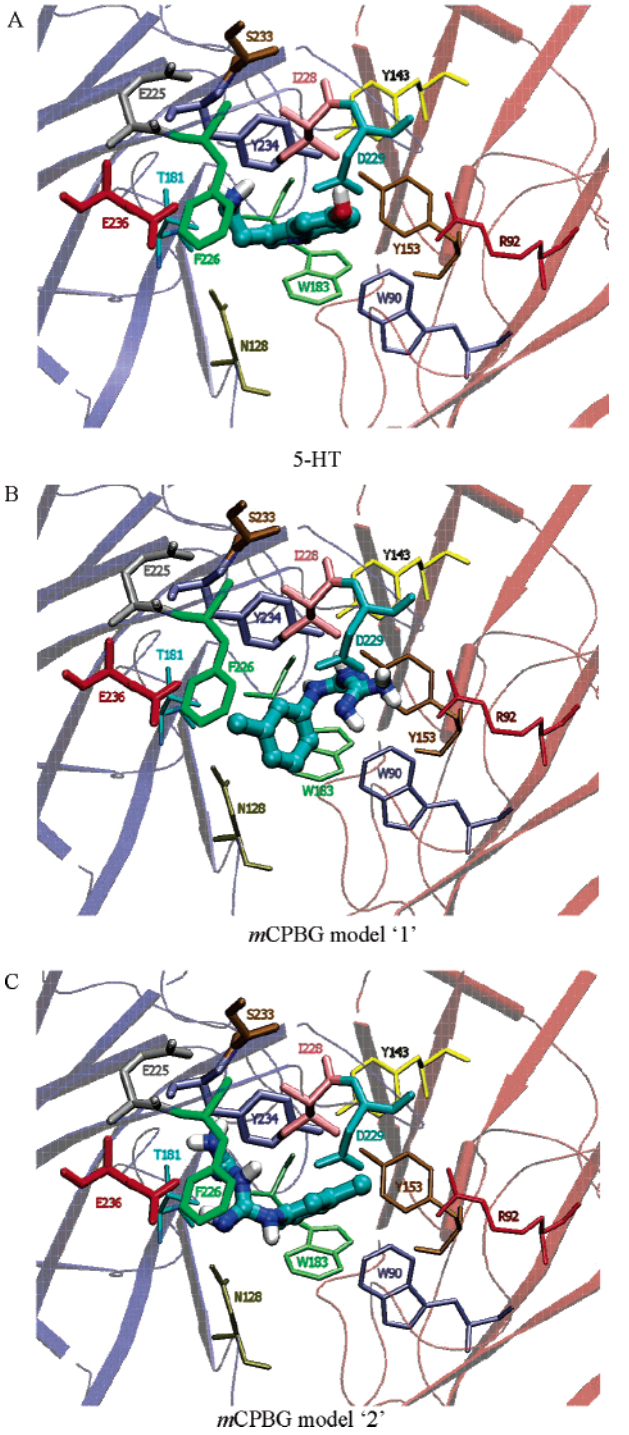

FIGURE 5: Docking of 5-HT and *m*CPBG to the murine 5-HT$_{3A}$R model. Modeling of the extracellular domain of the murine 5-HT$_{3A}$R and ligand docking were performed as described in Materials and Methods. Panel A shows the docked model of 5-HT. Two possible docked models were obtained for *m*CPBG and are shown as (B) model 1 and (C) model 2.

DISCUSSION

In this study, we have used a combination of biochemical, electrophysiological, and ligand docking studies to elucidate the role of loop C residues from the 5-HT$_{3A}$R in interaction with two agonists, 5-HT and *m*CPBG. The data are well corroborated by 5-HT and *m*CPBG docked receptor models. We have also determined partial agonist efficacies to elucidate the role of mutated amino acids in receptor gating. Mutation of four residues in loop C produced large changes in binding or functional parameters. Mutation of F226, I228, and D229 produced 5-HT selective effects for 5-HT versus *m*CPBG. F226 and I228 produced changes in agonist relative

Table 3: Docking Calculations for Models of 5-HT, 2-Me 5-HT, and *m*CPBG[a]

	N128	T179	T181	W183	F226	I228	D229	I230	S231	Y234	E236	W90	R92	Y153	I207
5-HT	+		+	PP	CP	+	HB		+	CP	SB	+		+	+
2-Me5-HT	+		+	PP	CP	+	HB	+	+	HB	SB	+		+	+
*m*CPBG1	+			CP	PP	+	SB	+	+	HB	+	+		HB	+
*m*CPBG2	+			PP	CP	+			+	CP	SB	+			

[a] Modeling of the extracellular domain of the murine 5-HT$_{3A}$R and ligand docking were performed as described in Materials and Methods. The results are also represented in Figure 5. Interactions predicted for 5-HT, 2-Me5-HT, and *m*CPBG (model 1 and model 2) are shown. Abbreviations: HB, hydrogen bond; SB, salt bridge; CP, cation$-\pi$ interaction; PP, $\pi-\pi$ interaction. A plus sign indicates within 4 Å of the docked ligand.

efficacies, whereas D229 is critical to 5-HT binding but not *m*CPBG binding. On the other hand, overall data for Y234 mutations support a role in both binding and gating.

Residues Involved in Mediating Binding and Gating by 5-HT. The docked model of 5-HT shows two aromatic residues, F226 and Y234, and two acidic residues, D229 and E236, from loop C participating in important interactions with 5-HT. A cation$-\pi$ interaction between F226 and 5-HT is indicated in the docked 5-HT model. Radioligand binding data for F226 mutations support this interaction. Electrophysiological data for F226A and F226Y receptors indicate that an aromatic residue at this position is required for agonist-induced channel opening. Changes in relative efficacy values support a role in gating. Thus, F226 appears to be important to 5-HT binding and subsequent gating of the receptor. The variability in the length of the C loop region of LGIC receptors produces gaps in the sequence alignment (Figure 1). However, F226 in the mouse 5-HT$_{3AS}$R is homologous to Y190 in the nACh α_7R, which has been shown to be important for binding and/or gating (*37*−*39*). In addition, crystal structures of the AChBP bound to carbamylcholine and nicotine indicate that a hydrogen bond is formed between the homologous residue (Tyr185) and Lys139 (loop B) in the ligand-bound conformation (*40*).

The D229A mutation produces a shift in both EC_{50} and K_i values for 5-HT but not for *m*CPBG. In addition, no changes in relative efficacy values were observed for D229A receptors. These data indicate a role for D229 in binding of 5-HT to the 5-HT$_{3AS}$R, but not in gating. This observation is supported by the docked 5-HT model which indicates a hydrogen bond between D229 and 5-HT. D229 is homologous to C193 in the mouse nAChR, which has been identified as being critical in the binding site of nAChR by photoaffinity labeling and mutagenesis studies (*41*−*43*). The homologous C188 in the AChBP crystal structure has been shown to be in contact with nicotine (*40*).

Mutation of Y234 to alanine ablated function. Immunofluorescence experiments indicate that this is probably due to a lack of cell surface expression. However, authors of a recent study reported that Y234A receptors were expressed on the cell surface (*8*). This difference could be due to expression levels below our level of detection or the use of different antisera in the mentioned study. The changes obtained in K_i and relative efficacy values indicate a role for Y234 in mediating binding and gating by 5-HT. In accordance with these results, docking studies show a cation$-\pi$ interaction between 5-HT and Y234. A recent crystal structure of the AChBP shows that the homologous residue (Y192) makes an aromatic contact with nicotine (*40*). Residues homologous to Y234 are strictly conserved as aromatic throughout the family (Figure 1). Separate lines of evidence have implicated the homologous Y198 in the nAChR in binding of acetylcholine and/or gating (*37*−*39*). The homologous Y205 in the β2 GABA$_A$R has been shown to be facing into the GABA binding pocket (*44*). Thus, data from multiple receptor types support a key role for Y234 in binding and gating mechanisms.

In addition to F226, D229, and Y234, the 5-HT docked model also indicates potential interactions with W183 and E236. There is strong evidence for a cation$-\pi$ interaction between the amino group of 5-HT and W183 (*45*). While our 5-HT docked model shows a $\pi-\pi$ interaction between 5-HT and W183, it should be noted that a small rotation of the carbon chain of 5-HT would realign the amino group, permitting a cation$-\pi$ interaction with W183. We hypothesize that the conformational mobility of the saturated carbon chain of 5-HT may allow a conformation in which the amino group is not salt bridged with E236 but forms a cation$-\pi$ interaction with W183. This mobility could play a role during the activation of the 5-HT$_3$R. E236 has been previously shown to be within 1 nm of the ligand binding site (*9*). Our 5-HT docked model corroborates this conclusion by showing a salt bridge between E236 and the amino group of 5-HT. E225 is another acidic residue which has been postulated to be involved in both binding and gating of the 5-HT$_3$R (*9*). Our partial agonist data support a role of E225 in gating. Since docking models do not support a binding interaction of E225 with any docked ligand, we propose that E225 may have a moderate involvement in gating, but not in ligand binding.

I228 appears to be selectively involved in 5-HT-mediated gating, as reflected by the changes in 5-HT-induced response characteristics, I_{max} values, and rank efficacy for the I228A mutation in comparison to the WT receptor. Interestingly, a similar phenomenon has been reported for the F129 residue from the 5-HT$_3$R (F107, according to the author's numbering) (*11*). The exact mechanism behind the 5-HT selective effect for I228 is unclear. Our docking studies show that I228 is within 4 Å of docked 5-HT and *m*CPBG and may interact with either ligand. However, an involvement in 5-HT-mediated gating is supported by experimental data. One explanation for the apparent discrepancy in docking and experimental data for I228 may be that this residue interacts with 5-HT in a conformation of 5-HT$_3$R that is different from the conformation represented by the docked model. I228 is also homologous to C192 of the mouse nAChR, which has been identified by photoaffinity labeling studies (*41*−*43*).

Interactions of mCPBG. The combined data suggest that *m*CPBG−5-HT$_3$R interactions are similar to 5-HT−5-HT$_3$R interactions, with D229 being a major point of difference. In ligand docking studies, two possible binding modes for *m*CPBG were obtained, with substantial differences in specific interactions. Model 1 (Figure 5B) predicts interactions of *m*CPBG with F226, D229, Y234, and Y153 (a loop

E residue). All of these interactions have been demonstrated for 5-HT but not for *m*CPBG. This model also shows an interaction with W183 (loop B). *m*CPBG interactions have been postulated by earlier studies for W183 and E236 (*9*, *10*). Although our data support the importance of both F226 and Y234 in *m*CPBG-mediated binding and gating, the data for D229 are unsupportive of model 1. In addition, although model 1 predicts the same interacting amino acids for both *m*CPBG and 5-HT, the nature of these interactions is different (Table 3). Specifically, model 1 predicts a cation$-\pi$ interaction between W183 and *m*CPBG and a $\pi-\pi$ interaction between W183 and 5-HT. This model also predicts a $\pi-\pi$ interaction between F226 and *m*CPBG, rather than the cation$-\pi$ interaction predicted between F226 and 5-HT. A salt bridge with D229 is predicted for *m*CPBG, while a hydrogen bond is indicated for 5-HT.

In contrast, model 2 (Figure 5C) predicts some differences in interacting amino acids, but for overlapping residues, the type of interaction for *m*CPBG is identical to that indicated for 5-HT (Table 3). With respect to our data, an important difference between models 1 and 2 is the interaction of D229 with *m*CPBG in model 1, but not in model 2. Model 2 accurately predicts a change in the binding affinity for 5-HT but not for *m*CPBG on D229A receptors. This difference is clearly supported by the biochemical data for D229A, suggesting that model 2 may best represent *m*CPBG$-$5-HT_3R binding. A second difference predicted by the model involves Y153 in loop E. We have previously reported that mutation of this residue also produces effects selective for 5-HT versus *m*CPBG (*46*). These data support the *m*CPBG model 2 (Figure 5C) for *m*CPBG$-$5-HT_3R interactions.

Final Conclusions. In addition to identification of loop C residues that are critical for receptor activation and ligand binding, results from this study identify molecular determinants of differential interaction of these two diverse agonists with loop C. Four key amino acids were identified as being important to ligand binding and/or gating of the receptor. Residues F226 and Y234 are important for both 5-HT and *m*CPBG interactions. I228 and D229 are specific for effects mediated by 5-HT compared to *m*CPBG, indicating a differential interaction of these ligands with loop C. Mutations at F226, I228, and Y234 also altered relative efficacies of agonists, suggesting a role in the gating mechanism. In support of a role in gating, a comparison of unliganded and liganded crystal structures of AChBP suggests that loop C undergoes the largest movement after agonist binding (*40*). A substituted cysteine accessibility method (SCAM) study of the loop C region of the β_2 $GABA_A$R also implicates this region in agonist-induced conformational changes (*44*).

Earlier studies of the 5-HT_{3A}R have shown that mutations of residues F129 of loop A (*11*) and Y153 of loop E (*46*) also show selectivity for 5-HT, but not for *m*CPBG. The results from our study, taken together with previous results, present an emerging picture of differential interactions of 5-HT and *m*CPBG with the murine 5-HT_{3A}R.

REFERENCES

1. Maricq, A. V., Peterson, A. S., Brake, A. J., Myers, R. M., and Julius, D. (1991) Primary structure and functional expression of the $5HT_3$ receptor, a serotonin-gated ion channel, *Science 254*, 432−437.
2. Costall, B., and Naylor, R. J. (2004) 5-HT_3 receptors, *Curr. Drug Targets: CNS Neurol. Disord. 3*, 27−37.
3. Arias, H. R. (2000) Localization of agonist and competitive antagonist binding sites on nicotinic acetylcholine receptors, *Neurochem. Int. 36*, 595−645.
4. Brejc, K., van Dijk, W. J., Klaassen, R. V., Schuurmans, M., van Der Oost, J., Smit, A. B., and Sixma, T. K. (2001) Crystal structure of an ACh-binding protein reveals the ligand-binding domain of nicotinic receptors, *Nature 411*, 269−276.
5. Le Novére, N., Grutter, T., and Changeux, J. P. (2002) Models of the extracellular domain of the nicotinic receptors and of agonist- and Ca^{2+}-binding sites, *Proc. Natl. Acad. Sci. U.S.A. 99*, 3210−3215.
6. Reeves, D. C., Sayed, M. F., Chau, P. L., Price, K. L., and Lummis, S. C. (2003) Prediction of 5-HT_3 receptor agonist-binding residues using homology modeling, *Biophys. J. 84*, 2338−2344.
7. Boess, F. G., Steward, L. J., Steele, J. A., Liu, D., Reid, J., Glencorse, T. A., and Martin, I. L. (1997) Analysis of the ligand binding site of the 5-HT_3 receptor using site directed mutagenesis: Importance of glutamate 106, *Neuropharmacology 36*, 637−647.
8. Price, K. L., and Lummis, S. C. (2004) The role of tyrosine residues in the extracellular domain of the 5-hydroxytryptamine$_3$ receptor, *J. Biol. Chem. 279*, 23294−23301.
9. Schreiter, C., Hovius, R., Costioli, M., Pick, H., Kellenberger, S., Schild, L., and Vogel, H. (2003) Characterization of the ligand-binding site of the serotonin 5-HT_3 receptor: The role of glutamate residues 97, 224, and 235, *J. Biol. Chem. 278*, 22709−22716.
10. Spier, A. D., and Lummis, S. C. (2000) The role of tryptophan residues in the 5-hydroxytryptamine$_3$ receptor ligand binding domain, *J. Biol. Chem. 275*, 5620−5625.
11. Steward, L. J., Boess, F. G., Steele, J. A., Liu, D., Wong, N., and Martin, I. L. (2000) Importance of phenylalanine 107 in agonist recognition by the 5-hydroxytryptamine$_{3A}$ receptor, *Mol. Pharmacol. 57*, 1249−1255.
12. Yan, D., Schulte, M. K., Bloom, K. E., and White, M. M. (1999) Structural features of the ligand-binding domain of the serotonin $5HT_3$ receptor, *J. Biol. Chem. 274*, 5537−5541.
13. Venkataraman, P., Venkatachalan, S. P., Joshi, P. R., Muthalagi, M., and Schulte, M. K. (2002) Identification of critical residues in loop E in the 5-HT_{3AS}R binding site, *BMC Biochem. 3*, 15.
14. Maksay, G., Bikádi, Z., and Simonyi, M. (2003) Binding interactions of antagonists with 5-hydroxytryptamine$_{3A}$ receptor models, *J. Recept. Signal Transduction Res. 23*, 255−270.
15. Hope, A. G., Belelli, D., Mair, I. D., Lambert, J. J., and Peters, J. A. (1999) Molecular determinants of (+)-tubocurarine binding at recombinant 5-hydroxytryptamine$_{3A}$ receptor subunits, *Mol. Pharmacol. 55*, 1037−1043.
16. Lankiewicz, S., Lobitz, N., Wetzel, C. H., Rupprecht, R., Gisselmann, G., and Hatt, H. (1998) Molecular cloning, functional expression, and pharmacological characterization of 5-hydroxytryptamine$_3$ receptor cDNA and its splice variants from guinea pig, *Mol. Pharmacol. 53*, 202−212.
17. Mochizuki, S., Miyake, A., and Furuichi, K. (1999) Identification of a domain affecting agonist potency of meta-chlorophenylbiguanide in 5-HT_3 receptors, *Eur. J. Pharmacol. 369*, 125−132.
18. Bartrup, J. T., and Newberry, N. R. (1996) Electrophysiological consequences of ligand binding to the desensitized 5-HT_3 receptor in mammalian NG108-15 cells, *J. Physiol. 490* (Part 3), 679−690.
19. Mott, D. D., Erreger, K., Banke, T. G., and Traynelis, S. F. (2001) Open probability of homomeric murine 5-HT3A serotonin receptors depends on subunit occupancy, *J. Physiol. 535*, 427−443.
20. van Hooft, J. A., and Vijverberg, H. P. (1997) Full and partial agonists induce distinct desensitized states of the 5-HT_3 receptor, *J. Recept. Signal Transduction Res. 17*, 267−277.
21. Joshi, P. R., Suryanarayanan, A., and Schulte, M. K. (2004) A vertical flow chamber for *Xenopus* oocyte electrophysiology and automated drug screening, *J. Neurosci. Methods 132*, 69−79.
22. Wu, C. H., Huang, H., Arminski, L., Castro-Alvear, J., Chen, Y., Hu, Z. Z., Ledley, R. S., Lewis, K. C., Mewes, H. W., Orcutt, B. C., Suzek, B. E., Tsugita, A., Vinayaka, C. R., Yeh, L. S., Zhang, J., and Barker, W. C. (2002) The Protein Information Resource: An integrated public resource of functional annotation of proteins, *Nucleic Acids Res. 30*, 35−37.
23. Thompson, J. D., Higgins, D. G., and Gibson, T. J. (1994) CLUSTAL W: Improving the sensitivity of progressive multiple sequence alignment through sequence weighting, position-specific gap penalties and weight matrix choice, *Nucleic Acids Res. 22*, 4673−4680.

24. Xiang, Z., and Honig, B. (2001) Extending the accuracy limits of prediction for side-chain conformations, *J. Mol. Biol. 311*, 421−430.
25. Xiang, Z., Soto, C. S., and Honig, B. (2002) Evaluating conformational free energies: The colony energy and its application to the problem of loop prediction, *Proc. Natl. Acad. Sci. U.S.A. 99*, 7432−7437.
26. Laskowski, R. A., MacArthur, M. W., Moss, D. S., and Thornton, J. M. (1993) PROCHECK: A program to check the stereochemical quality of protein structures, *J. Appl. Crystallogr. 26*, 283−291.
27. McDonald, I. K., and Thornton, J. M. (1994) Satisfying hydrogen bonding potential in proteins, *J. Mol. Biol. 238*, 777−793.
28. Morris, G. M., Goodsell, D. S., Hallaway, R. S., Huey, R., Hart, W. E., Belew, R. K., and Olson, A. J. (1998) Automated Docking Using a Lamarckian Genetic Algorithm and Empirical Binding Free Energy Function, *J. Comput. Chem. 19*, 1639−1662.
29. Cornell, W. D., Cieplak, P., Bayly, C. I., Gould, I. R., Merz, K. M. J., Ferguson, D. M., Spellmeyer, D. C., Fox, T., Caldwell, J. W., and Kollman, P. A. (1995) A second generation force field for the simulation of proteins, nucleic acids, and organic molecules, *J. Am. Chem. Soc. 117*, 5179−5197.
30. Colquhoun, D. (1998) Binding, gating, affinity and efficacy: The interpretation of structure−activity relationships for agonists and of the effects of mutating receptors, *Br. J. Pharmacol. 125*, 924−947.
31. Downie, D. L., Hope, A. G., Belelli, D., Lambert, J. J., Peters, J. A., Bentley, K. R., Steward, L. J., Chen, C. Y., and Barnes, N. M. (1995) The interaction of trichloroethanol with murine recombinant 5-HT_3 receptors, *Br. J. Pharmacol. 114*, 1641−1651.
32. Downie, D. L., Hall, A. C., Lieb, W. R., and Franks, N. P. (1996) Effects of inhalational general anaesthetics on native glycine receptors in rat medullary neurones and recombinant glycine receptors in *Xenopus* oocytes, *Br. J. Pharmacol. 118*, 493−502.
33. O'Shea, S. M., and Harrison, N. L. (2000) Arg-274 and Leu-277 of the γ-aminobutyric acid type A receptor α2 subunit define agonist efficacy and potency, *J. Biol. Chem. 275*, 22764−22768.
34. O'Shea, S. M., Wong, L. C., and Harrison, N. L. (2000) Propofol increases agonist efficacy at the $GABA_A$ receptor, *Brain Res. 852*, 344−348.
35. Rajendra, S., Lynch, J. W., Pierce, K. D., French, C. R., Barry, P. H., and Schofield, P. R. (1995) Mutation of an arginine residue in the human glycine receptor transforms β-alanine and taurine from agonists into competitive antagonists, *Neuron 14*, 169−175.
36. Lynch, J. W. (2004) Molecular structure and function of the glycine receptor chloride channel, *Physiol. Rev. 84*, 1051−1095.
37. Akk, G., Zhou, M., and Auerbach, A. (1999) A mutational analysis of the acetylcholine receptor channel transmitter binding site, *Biophys. J. 76*, 207−218.
38. O'Leary, M. E., and White, M. M. (1992) Mutational analysis of ligand-induced activation of the *Torpedo* acetylcholine receptor, *J. Biol. Chem. 267*, 8360−8365.
39. Tomaselli, G. F., McLaughlin, J. T., Jurman, M. E., Hawrot, E., and Yellen, G. (1991) Mutations affecting agonist sensitivity of the nicotinic acetylcholine receptor, *Biophys. J. 60*, 721−727.
40. Celie, P. H., van Rossum-Fikkert, S. E., van Dijk, W. J., Brejc, K., Smit, A. B., and Sixma, T. K. (2004) Nicotine and carbamylcholine binding to nicotinic acetylcholine receptors as studied in AChBP crystal structures, *Neuron 41*, 907−914.
41. Dennis, M., Giraudat, J., Kotzyba-Hibert, F., Goeldner, M., Hirth, C., Chang, J. Y., Lazure, C., Chretien, M., and Changeux, J. P. (1988) Amino acids of the *Torpedo marmorata* acetylcholine receptor α subunit labeled by a photoaffinity ligand for the acetylcholine binding site, *Biochemistry 27*, 2346−2357.
42. Kao, P. N., Dwork, A. J., Kaldany, R. R., Silver, M. L., Wideman, J., Stein, S., and Karlin, A. (1984) Identification of the α subunit half-cystine specifically labeled by an affinity reagent for the acetylcholine receptor binding site, *J. Biol. Chem. 259*, 11662−11665.
43. Mishina, M., Tobimatsu, T., Imoto, K., Tanaka, K., Fujita, Y., Fukuda, K., Kurasaki, M., Takahashi, H., Morimoto, Y., Hirose, T., et al. (1985) Location of functional regions of acetylcholine receptor α-subunit by site-directed mutagenesis, *Nature 313*, 364−369.
44. Wagner, D. A., and Czajkowski, C. (2001) Structure and dynamics of the GABA binding pocket: A narrowing cleft that constricts during activation, *J. Neurosci. 21*, 67−74.
45. Beene, D. L., Brandt, G. S., Zhong, W., Zacharias, N. M., Lester, H. A., and Dougherty, D. A. (2002) Cation-π interactions in ligand recognition by serotonergic (5-HT3A) and nicotinic acetylcholine receptors: The anomalous binding properties of nicotine, *Biochemistry 41*, 10262−10269.
46. Joshi, P. R., Suryanarayanan, A., Bikadi, Z., Muthalagi, M., Trupti, K. R., Gaines, C., and Schulte, M. K. (2004) in *Society for Neuroscience Abstracts*, San Diego.

BI050661E